Case Studies in Thermal Engineering 39 (2022) 102390

Contents lists available at ScienceDirect

Case Studies in Thermal Engineering

journal homepage: www.elsevier.com/locate/csite

On heat and flow characteristics of Carreau nanofluid and tangent hyperbolic nanofluid across a wedge with slip effects and bioconvection☆

Irfan Saif Ud Din [a], Imran Siddique [a,*], Rifaqat Ali [b], Fahd Jarad [c,d,**], Sohaib Abdal [e,f], Sajjad Hussain [g]

[a] Department of Mathematics, University of Management and Technology, Lahore, 54770, Pakistan
[b] Department of Mathematics, College of Science and Arts, King Khalid University, Muhayil, 61413, Abha, Saudi Arabia
[c] Department of Mathematics, Cankaya University, Etimesgut, Ankara, 06790, Turkey
[d] Department of Medical Research, China Medical University Hospital, China Medical University, Taichung, 40402, Taiwan
[e] School of Mathematics, Northwest University, No.229 North Taibai Avenue, Xi'an, 7100069, China
[f] Department of Mathematics, Khwaja Fareed University of Engineering and Information Technology, Rahim Yar Khan, Pakistan
[g] School of Aerospace and Mechanical Engineering, Nanyang Technological University, Singapore

ARTICLE INFO

Keywords:
Carreau fluid
Tangent hyperbolic fluid
Nanofluid
Magnetohydrodynamics
Bioconvection
Runge-Kutta scheme

ABSTRACT

We scrutinized the influence of nonlinear heat radiation on heat transmission evaluation of Carreau nanofluid and tangent hyperbolic nanofluid streams across a wedge with gyrotactic microorganisms by taking slip situations into consideration in this research article. The necessary nonlinear partial differential formulation is transmuted into non-linear ordinary differential equations by employing appropriate similarity variables, and these equations, including the boundary constraints are resolved in Matlab software utilizing Runge-Kutta fourth order via shooting tactic. A definite description of the framework is achieved by fluctuating the inputs of influential variables of the dependent functions and exhibited via graphs. The inhibiting flow velocity is portrayed by the intensifying inputs of buoyancy ratio, magnetic force, Rayleigh number, and eigenvalue. As a consequence of thermophoresis and Brownian motion of nanoparticles, the temperature of the liquids initiates to ascend instantly. Because of differentiated viscous effects, the flow velocity for Carreau nanofluid is slower than that of tangent hyperbolic fluid and the temperature behavior is reversed. Further, the magnitude of skin friction factor for tangent hyperbolic nanofluid is almost half ofs that of Carreau nanofluid.

Nomenclature

List of Symbols

u, v	velocity components
(x, y)	Direction along and perpendicular to the wedge
u_w	velocity of the wall

☆ Fully documented templates are available in the elsarticle package on CTAN.

* Corresponding author.
** Corresponding author. Department of Mathematics, Cankaya University, Etimesgut, Ankara, 06790, Turkey.
E-mail addresses: imransmsrazi@gmail.com (I. Siddique), fahd@cankaya.edu.tr (F. Jarad).

https://doi.org/10.1016/j.csite.2022.102390
Received 11 July 2021; Received in revised form 23 August 2022; Accepted 26 August 2022
Available online 13 September 2022

u_e	velocity of the far flow
u_∞	velocity of mainstream
θ_w	temperature ratio parameter
B_o	magnetic field strength
C	concentration of nanoparticles
T	temperature of nanoparticles
N	Micro-organisms distribution
g	gravity
n	power law index
K^*	mean absorption co-efficient
k	thermal conductivity
C_p	specific heat at constant pressure
D_B	Brownian diffusion coefficient
D_T	thermophoresis diffusion coefficient
D_m	diffusivity of microrganisms
T_∞	ambient temperature
C_∞	ambient concentration of nanoparticles
N_∞	ambient micro-organisms distribution
τ	relaxation time of heat flux
τ_w	shear stress
Q_o	heat source/sink coefficient
m	fitted rate parameter
Ea	activation energy
b	chemotaxis constant
W_c	speed of gyrotactic cell
n_1	rotation of micro-organisms
q_w	wall heat flux
M	magnetic field parameter
k_f	Thermal conductivity of basefluid
t	time
Pr	Prandtl number
Nb	Brownian motion parameter
Nt	thermophoresis parameter
Q	heat source
E	activation energy coefficient
Lb	bio-convection Lewis number
Pe	Peclet number
C_1	chemical reaction parameter
T_w	wall constant temperature
C_w	nanoparticles concentration at wall
W_e	Local Weissenberg number
f	dimensionless stream function
S	similarity concentration of nanoparticles
V_o	suction Parameter
C_f	Skin friction coefficient
Sh_x	Sherwood number
Nu_x	Nusselt number
Re_x	Local Reynolds

Greek Symbols

α	thermal diffusivity of base fluid
μ	viscosity of fluid
ψ	stream function
β^*	Deborah number
β	concentration slip parameter
ν	kinematic viscosity
λ	velocity slip parameter
σ	electrical conductivity
σ^*	Stefan-Boltzmann constant
ρ	Density
ρ_p	Nanoparticle Mass density

γ^*	average volume of microorganisms
γ_w	wedge angle
γ	Eigen value
ω	mixed convection parameter
η	similarity variable
θ	similarity temperature
χ	similarity density of micro-organisms
ξ	thermal slip parameter
Γ	material parameter
δ	temperature difference
Ω_B	microorganisms concentration difference

Subscripts

p	nanoparticles
w	on the sheet surface
∞	condition for away cone surface
f	base fluid
nf	nanofluid

1. Introduction

The survey of non-Newtonian fluids has attracted considerable interest in the research field in current decades. The analysis of these fluids is encouraged by their significance in industry sectors like material processing, plastic thawing, pharma products, polymeric liquids, biochemical engineering, toxin and nuclear plants, mechanical applications, and the food industry. Some prestigious examples signify the blood, honey, perfumes, glue, diesel fuel, asphalts, cream, and so even more. Tangent hyperbolic fluid is viewed as a fluid with shear thinning/thickening and normal stress interaction. Numerous scholars often use tangent hyperbolic models with diverse flow features because of their fascinating rheological characteristics. Ramzan et al. [1] debated the fluid motion of a 3-D tangent hyperbolic nano-fluid flow. Khan et al. [2] identified a nominal impact of radiation and chemical reaction on tangent hyperbolic fluid flow. Khaled et al. [3] discussed the bio-convection flow of tangent hyperbolic nano-liquid. Kumar et al. [4] studied the flow of tangent hyperbolic fluid passing over a stretching sheet. Gharami et al. [5] discussed the time-dependent MHD flow of tangent hyperbolic nanofluid. Oyelakin et al. [6] utilized the spectral method to initiate a thermo-physical interpretation of the three-dimensional magneto-hydrodynamic flow of a tangent hyperbolic nanofluid. Ullah et al. [7] implemented the Lie group analysis with the shooting technique of MHD incompressible flow of tangent hyperbolic fluid. Karthik et al. [8] used nonlinear radiation, swimming microbes, and nanoparticles to study 3D bioconvective viscoelastic nanofluid movement across a heated Riga surface. Mariam et al. [9] used the Runge-Kutta scheme to investigate the effect of gyrotactic microorganisms on non-Newtonian liquid (Maxwell fluid) passing over an expanding cylindrical surface. Siddique et al. [10] investigated a conceptual framework for tangent hyperbolic liquid of nano-biofilm due to an elongating or contracting sheet, which includes a point of stagnation flow, and chemical reaction with activation energy, and gyrotactic microbe bioconvection.

Several researchers have focused on non-Newtonian fluids in the recent past. The Carreau fluid model is a non-Newtonian fluid model that delivers a fundamental relationship between low shear rate (which behaves as Newtonian fluid) and higher shear rates (acts as power law fluid). Such fluids could be identified in toothpaste, molten polymers, animal blood, pulps, as well as other components. Many investigators analyzed the behavior of a Carreau fluid in respective morphologies. Khan et al. [11] perceived the heat and mass designation in non-axisymmetric Homann stagnation point flow occasioned by a linear squeezed sheet in the existence of a permeable material. Noreen et al. [12] noticed the influence of heat transfer of Carreau fluid flow on an inclined asymmetric. Khan et al. [13] observed the wall slip characteristics of Carreau fluid flow on the movable boundary layer. Nazir et al. [14] studied the effects of Cattaneo–Christov heat flux model of Carreau fluid and many other scholars [15–18].

Bio-convection is a captivating liquid notion occasioned by the gliding of microbes. Bio-convection is a strategy wherein slight density microorganisms dive at the edge of a fluid, inflicting unorganized configurations and destabilization. Since they dive in the upper portion, such gyro-tactic motile microorganisms, such as algae, are more probable to gather across an upper fluid layer that would be a root of a volatile upper part, ensuing in more saturated stratification. The motion of gyro-tactic microorganisms is infinitesimal (convection), whereas the bio-convection technique is on a much more massive scale. The density of the base fluid boosts due to bio-convection occasioned by the automotive rotation of microbes in a particular pattern in the base fluid that interacts spatially with predefined stimulants. Gyro-tactic microorganisms are utilized in nanoparticles to strengthen fluid blending since they are culpable for the bio-convection methodology. Such microbes are coarser than water and typically swim in a chaotic fashion. This notion has recently garnered considerable interest since it has a great deal of realistic implementations in biotechnology, bio-microsystems, and bio-sciences. Bio-convection is meaningful in the filtering of microbial oil as well as in meteorological phenomena like hot springs conquered by motile micro-organisms referred to as thermopiles. Abdelmalek et al. [19] presented a theoretical model for Williamson nano-fluid bio-convection flow. Ullah and Jang [20] addressed the existence of nano-sized molecules with gyrotactic motile microbes. Habib et al. [21] probed the theoretical and mathematical characteristics of Maxwell micropolar

nanoparticles with diluted homogeneous nanoparticles and gyrotactic microbe diffusion. Abdal et al. [22] investigated the effects of activation energy and different transit variables on two-dimensional stagnation point movement of a nano-biofilm containing gyrotactic microbes across a porous straining/shrinking sheet. Abdal et al. [23] studied the effects of magnetohydrodynamic Williamson Sutterby nanoparticles caused by a rotating cone with bioconvection and anisotropic slip. Habib et al. [24] examined the dynamics of electric current factors, heat radiation, activation energy, mass and heat transformation of a magnetic flowing fluid containing nanomaterials and motile microbes over a porous extending sheet. Abdal et al. [25] investigated the role of multi-slips and bioconvection in the transpiration of micropolar nanomaterials through porous material over an extending sheet in PST and PHF environments. The few aspects of bio-convection flow have perceived by some authors [26,27].

In a huge series of nuclear and thermal-hydraulic mechanisms, heat transport incorporating fluid flow is mandated. A diversity of fluids and operational parameters are being inspected in order to optimize the heat transportation procedures. Solar power merchants, nuclear reactor cooling, living thing transpiration, oil and gas engineering, enriched oil recovery, agricultural production, and biomechanics are indeed a few of the substantial implementations. Numerous evaluations on the commuting of heat and mass in Newtonian and non-Newtonian fluids are being implemented over the last couple of years. Consequently, a few current surveys are debated here. Koyama et al. [28] debated how to enhance the thermal reliability of a hydrate-based heat engine. Wang et al. [29] initiated an innovative strategy for aligning multiple heat sources. Couvreur et al. [30] developed a scheme for employing residual heat from burning fuel. Jury et al. [31] revealed the transformation mechanisms in a super-elastic nickel-titanium SMA wire that had been confined to a force-controlled incredibly tensile cycle. Wang et al. [32] examined the thermal allocation for transportation of Darcy-Forchheimer Maxwell Sutterby nanofluid flow with the presence of Cattaneo-Christov heat transformation and electromagnetic field. Abdal et al. [33] researched the heat transport for bioconvective movement of Maxwell nanoparticles over a stretching/shrinking sheet with Cattaneo-Christov flux using a fourth-order Runge-Kutta procedure with a shooting method.

Radiation is a sort of energy transfer that has a vast scope of utilization notably in the solar industry. This type of heat transfer does not necessitate the use of a material medium. The consequence of thermal radiation has piqued the appreciation of several scholars probably due to its innumerable implementations in polymer manufacturing techniques. Besides this, nano-liquids are perceived as one of the most efficacious refrigerant liquids in industries such as transportation, microelectronics, optical, and manufactured goods. Raisi et al. [34] reviewed the evaluation of circular and ellipsoidal vanes in a square chamber subject to radiation implications under heat transfer of nanoparticles. Ali et al. [35] examined Newtonian nano-fluid flow embodied with thermal radiation and heat generation/absorption temperature oriented over a stretching cylinder which was numerically, tackled using the Runge–Kutta Fehlberg method with a shooting system. Tamilzharasan et al. [36] investigated the Williamson nanofluid using the double Cattaneo-Christov theory, radiation, dual stratification, and the effect of activation energy. Habib et al. [37] was credited with various characteristics of Sisko nanoparticles flow over-stretching cylinder and bioconvection of motile microbes in the presence of activation energy and non-Fourier thermal diffusion. Certain nominated articles highlighting the pertinence of thermal radiation are outlined as [38–40].

In the early 1930's, Falkner and Skan scrutinized flow over a static wedge. Afterward that year, in 1937, Hartree [41] investigated the solution's reliance on the wedge angle parameter. Flows over wedge moulded substrates are an impactful area of analysis since they are witnessed in a wide range of scientific and industrial prosecutions such as hydrodynamics, engine performance, magneto-hydrodynamics, geothermal systems. Kebede et al. [42] ascertained the influence of heat and mass transportation of time dependent tangent hyperbolic nanofluid. Hamid et al. [43] deliberated the time dependent stagnation-point flow effects of Williamson nano-fluid across a static/moving wedge. Siavashi and Iranmehr [44] evaluated two-phase mixture model of nanofluid. Sreedevi et al. [45] done a comparative study of hybrid nanofluid by using Galarkin method.

A glance at the review of literature reveals that no comparative analysis is attempted for Buongiorno's model nanofluid mass and heat transmission attributes of Carreau nanofluid and tangent hyperbolic nanofluid across a wedge with slip aspects. Jyothi et al. [46] assessed the effect of variable thermal conductivity on heat transition analysis of the Carreau nanofluid stream past a wedge by carrying slip conditions into consideration. However, in their exploration, they did not take into account the tangent hyperbolic nanofluid, porous medium, motile density of microorganisms, heat source and chemical reaction with activation energy. The purpose and novelty of current research are to evaluate the stream and heat transportation of Carreau and tangent hyperbolic nanofluids with gyrotactic microbes under slip conditions over a wedge to bridge the gap. The numerical simulation of transformed leading equations is acquired by incorporating the fourth-order R–K technique with the shooting strategy. The influences of encoded parameters on the velocity, temperature, nanoparticle concentration and motile density of micro-organism profiles for the two flow models are graphically exhibited. Physically, this can be use in industry sectors like the material processing, plastic thawing, pharma products, polymeric liquids, biochemical engineering, toxin and nuclear plants, mechanical applications, and food industry. Also can be seen in blood, honey, perfumes, glue, diesel fuel, asphalts, cream, and so even more. Such fluids could be identified in tooth paste, molten polymers, animal blood, pulps, as well as other components. This can also applied in the implementations in biotechnology, bio-microsystems, and bio-sciences .

2. Physical model and mathematical formulation

We perceive a two-dimensional, steady MHD laminar boundary layer stream of Carreau fluid and tangent hyperbolic fluid of density ρ_{nf} over a wedge with stretching velocity u_w and free stream velocity u_e. The wedge angel is $\Omega = \gamma\pi$. Our modification designates the fundamental equation of continuity, velocity equation, temperature equation, concentration equation and gyrotactic microorganisms equation in Cartesian coordinate system with incorporation of activation energy, thermal radiation and a heat source. Choose the positive $x - axis$ that is quantified across the wedge's substrate, whereas the $y - axis$ is orthogonal to the wedge's substrate velocity component. In y-direction, magnetic field of intensity B_0 is subjected. The configuration of physical situations is mapped in Fig. 1.

A Carreau liquid's constitutive model or non-Newtonian viscosity is described by:

$$\tau = -pI + S + \mu(\dot{\gamma})A_1, \mu = \mu_\infty + (\mu_0 - \mu_\infty)\left[1 + (\Gamma\dot{\gamma})^2\right]^{\frac{n-1}{2}}.$$

Here, p is the pressure, I denotes the identity tensor, A_1 represents the first Rivlin-Erickson tensor, μ_0 and μ_∞ are the zero and unbounded shear rate viscosities, n indicates the power law index, C is a material time factor and G is specified as:

$$\dot{\gamma} = \sqrt{\frac{1}{2}\Pi}, \qquad \Pi = trace(A_1^2),$$

here, P denotes the second invariant strain tensor.

The power-law index depicts fluid movement and fluid is classified as shear thinning for $0 < n < 1$, shear thickness for $n > 1$, Newtonian fluid for $n = 1$ and/or $\Gamma = 0$ and the power-law concept can be achieved for high values of Γ. The viscosity values at zero and unlimited shear rates were fixed to 1 and 0.001, respectively. As a consequence, the perceived viscosity *mu* for the Carreau fluid model can be written as:

$$\mu = \mu_0\left[\beta^* + (1-\beta^*)\left[1 + (\Gamma\dot{\gamma})^2\right]^{\frac{n-1}{2}}\right],$$

where, $\beta^* = \frac{\mu_\infty}{\mu_0}$ denotes the non-dimensional ratio of infinity shear-rate viscosity to zero shear-rate viscosity, assumed to be lower than one.

Tangent hyperbolic fluid has the following constitutive model:

$$\bar{\tau} = [\mu_\infty + (\mu_0 + \mu_\infty)\tanh\,(\Gamma\bar{\dot{\gamma}})^n]\bar{\dot{\gamma}},$$

wherein, $\bar{\tau}$ is the excessive stress tensor, μ_∞ represents the infinity shear rate viscosity, μ_0 denotes the zero shear rate viscosity, Γ is the time varying material constant, n indicates the power law index, also termed as the flow pattern index, and $\bar{\dot{\gamma}}$ is stated as:

$$\bar{\dot{\gamma}} = \sqrt{\frac{1}{2}\sum_i\sum_j \bar{\dot{\gamma}}_{ij}\bar{\dot{\gamma}}_{ji}} = \sqrt{\frac{1}{2}\Pi},$$

where, $\Pi = \frac{1}{2}tr(gradV + (gradV)^T)^2$. We examine Eq. (2.22) for the scenario when $\mu = 0$ since it is unable to analyze the topic for infinite shear rate viscosity and because we are examining Tangent hyperbolic fluid that exhibits shear thinning impacts, so $\Gamma\bar{\dot{\gamma}} < 1$. Then Eq. (2.22) has the following form:

$$\begin{aligned}\bar{\tau} = \quad & \mu_0[(\Gamma\bar{\dot{\gamma}})^n]\bar{\dot{\gamma}} = \mu_0[(1 + \Gamma\bar{\dot{\gamma}} - 1)^n]\bar{\dot{\gamma}} \\ & = \mu_0[1 + n(\Gamma\bar{\dot{\gamma}} - 1)]\bar{\dot{\gamma}}.\end{aligned}$$

The energy efficiency equation asserts that the system's entire energy is preserved. In the elimination of radiation and dispersion, mathematically we have

$$\rho c_p\frac{dT}{dt} = -\nabla \bullet q,$$

here, q is the thermal heat rate. According to Fourier's law

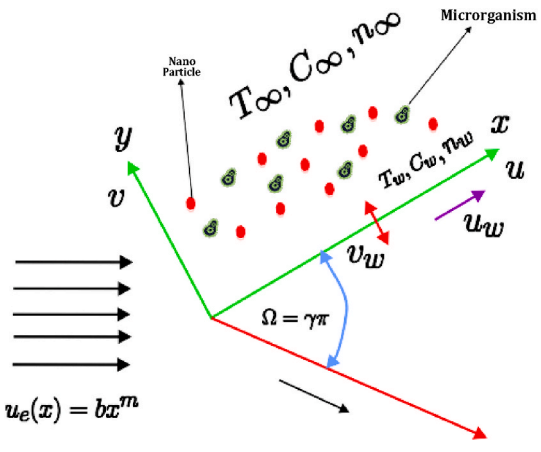

Fig. 1. Problem description.

$$q = -k\nabla T$$

As a result, the energy equation is transformed into

$$\rho c_p \frac{dT}{dt} = k\nabla^2 T$$

Leading formulation for boundary layer incompressible flows are [46,47]:

$$\frac{\partial u}{\partial x} + \frac{\partial v}{\partial y} = 0, \tag{1}$$

$$u\frac{\partial u}{\partial x} + v\frac{\partial u}{\partial y} = u_e\frac{du_e}{dx} + \nu\frac{\partial^2 u}{\partial y^2}\left(1 + \Gamma_C^2\left(\frac{\partial u}{\partial y}\right)^2\right)^{\frac{n-1}{2}} + \nu(n-1)\Gamma_C^2\frac{\partial^2 u}{\partial y^2}\left(\frac{\partial u}{\partial y}\right)^2 \tag{2}$$

$$\left(1 + \Gamma_C^2\left(\frac{\partial u}{\partial y}\right)^2\right)^{\frac{n-3}{2}} + \nu(1-\varepsilon)\frac{\partial^2 u}{\partial y^2} + \sqrt{2}\nu\Gamma_T\varepsilon\frac{\partial u}{\partial y}\frac{\partial^2 u}{\partial y^2} - \frac{\sigma_{nf}}{\rho_{nf}}\left(B_0^2 - \frac{\nu}{k}\right)\left(u - u_e\right)$$

$$+\left(\frac{1}{\rho_f}\right)\left[(1-C_\infty)\rho_f\beta^*(T-T_\infty) - (\rho_p - \rho_f)g(C-C_\infty) - (n-n_\infty)g\gamma^*(\rho_m - \rho_f)\right],$$

$$u\frac{\partial T}{\partial x} + v\frac{\partial T}{\partial y} = \frac{k}{\rho_{cp}}\frac{\partial^2 T}{\partial y^2} + \tau\left[D_B\frac{\partial C}{\partial y}\frac{\partial T}{\partial y} + \frac{D_T}{T_\infty}\left(\frac{\partial T}{\partial y}\right)^2\right] - \frac{1}{\rho C_p}\frac{\partial q_r}{\partial y} + Q_0(T - T_\infty), \tag{3}$$

$$u\frac{\partial C}{\partial x} + v\frac{\partial C}{\partial y} = D_B\frac{\partial^2 C}{\partial y^2} + \frac{D_T}{T_\infty}\frac{\partial^2 T}{\partial y^2} - (Kr)^2(C - C_\infty)\left(\frac{T}{T_\infty}\right)^m exp\left(\frac{-E_a}{K_1 T}\right), \tag{4}$$

$$u\frac{\partial n}{\partial x} + v\frac{\partial n}{\partial y} = -\frac{bW_c}{(C_w - C_\infty)}\frac{\partial}{\partial y}\left(n\frac{\partial C}{\partial y}\right) + D_m\frac{\partial}{\partial y}\frac{\partial n}{\partial y}. \tag{5}$$

along with the boundary conditions [46],

$$\left.\begin{aligned} u = L\frac{\partial u}{\partial y},\ v = v_w, w = 0,\ T = T_w + k_1\frac{\partial T}{\partial y},\ C = C_w + k_2\frac{\partial C}{\partial y},\ n = n_w,\quad as\ y = 0, \\ u \to\ u_e = bx^m, T \to\ T_\infty, C \to\ C_\infty, n \to\ n_\infty,\quad as\ y \to \infty. \end{aligned}\right\} \tag{6}$$

Consider the following similarity transformation in order to modify Eqs. (1)–(6) [?].

$$\psi = \sqrt{\frac{2\nu b}{m-1}}x^{\frac{m+1}{2}}f(\eta), \eta = \sqrt{\frac{b(m+1)}{2\nu}}x^{\frac{m-1}{2}}y, \theta(\eta) = \frac{T - T_\infty}{T_w - T_\infty}, \varphi(\eta) = \frac{C - C_\infty}{C_w - C_\infty}, \chi(\eta) = \frac{n - n_\infty}{n_w - n_\infty}. \tag{7}$$

The non-linear partial differential variables (2)–(5) are transformed into a system of corresponding ODE's by utilization of expression (7).

$$\left[\left(1 + We^2 f'\prime^2\right)^{\frac{n-3}{2}}\left(1 + nWe^2 f'\prime^2\right) + (1-\varepsilon) + \frac{\varepsilon}{\sqrt{2}}(2-\gamma)W_T f'\prime\right]f'\prime' \tag{8}$$

$$+ff'\prime + \gamma(1 - f'2) - M(f' - 1) + \omega(\theta - NrS - Rb\chi) = 0,$$

$$\theta'\prime + Prf\theta' + PrNb\theta'\varphi' + PrNt\theta'2$$

$$+\frac{4}{3R}[1 + \theta(\theta_w - 1)]^3\theta'\prime + \frac{4}{R}[1 + \theta(\theta_w - 1)]^2\theta'2 + PrQ\theta = 0, \tag{9}$$

$$\varphi'\prime + Lef\varphi' + \left(\frac{Nt}{Nb}\right)\theta'\prime - C_1\varphi(1 + \delta\theta)^m exp\left(\frac{-E}{1 + \delta\theta}\right) = 0, \tag{10}$$

$$\chi'\prime + Lb(f\chi') - Pe[S'\prime(\chi + \Omega_B) + \chi' S'] = 0. \tag{11}$$

The transformed boundary conditions are:

$$\left.\begin{aligned} f(0) = V_0,\ f'(0) = \lambda f''(0),\ \theta(0) = 1 + \xi\theta'(0),\ S(0) = 1 + \beta S'(0),\ \chi(0) = 1,\quad at\ \eta = 0, \\ f'(\infty) \to 1,\ \theta(\infty) \to 0,\ S(\infty) \to 0,\ \chi(\infty) \to 0,\ as\ \eta \to \infty. \end{aligned}\right\} \tag{12}$$

The dimensionless parameters are: $Pr = \frac{\mu_{cf}}{k}$, $Nt = \frac{\rho_{cp}D_T(T_w - T_\infty)}{\nu\rho_{cf}T_\infty}$, $N_b = \frac{\rho_{cp}D_B(C_w - C_\infty)}{\nu\rho_{cf}}$, $\theta_w = \frac{T_w}{T_\infty}$, $L_e = \frac{V}{D_B}$, $M = \frac{\sigma B_o^2}{2w_1\rho_f}$, $R = \frac{16T_\infty^3\sigma^*}{3K^*k_f}$, $\gamma = \frac{2m}{m+1}$, $\omega =$

$\frac{2\beta^* g(1-C_\infty)(T_w-T_\infty)}{b^2(m+1)x^{2m-1}}$, $W_e = \left(\frac{b^3\Gamma_C^2(m+1)x^{3m-1}}{2\nu}\right)^{\frac{1}{2}}$, $Q = \frac{2Q_o}{b(m+1)x^{m-1}}$, $E = \frac{E_a}{k_1 T_\infty}$, $\delta = \frac{(T_w-T_\infty)}{T_\infty}$, $W_T = \left(\frac{b^3\Gamma_T^2(m+1)x^{3m-1}}{2\nu}\right)^{1/2}$, $\beta_T = \frac{2m}{m+1}$, $C_1 = \frac{2\nu(k_r)^2}{D_B b(m+1)x^{m-1}}$.

3. Physical quantities

3.1. Surface drag force

Skin Friction for Carreau Fluid:
The skin friction coefficient is defined as

$$Cf_x = \frac{\tau_w}{\rho U_e^2/2}$$

where, τ_w signify shear stress and is defined as

$$\tau_w = \mu_0 \frac{\partial u}{\partial y}\left[\left[1+\Gamma_C^2\left(\frac{\partial u}{\partial y}\right)^2\right]^{\frac{n-1}{2}}\right] \; at \; y = 0$$

Thus

$$Cf_x(Re_x)^{-\frac{1}{2}} = \frac{2}{\sqrt{2-\beta}} f'\prime(0)[1+We^2(f'\prime(0))^2]^{\frac{n-1}{2}}$$

Skin Friction for Tangent Hyperbolic Fluid:
The skin friction coefficient is defined as

$$Cf_x = \frac{\tau_w}{\rho U_w^2}$$

where, τ_w signify shear stress and is defined as

$$\tau_w = \left[\left(1-\varepsilon\right)\frac{\partial u}{\partial y} + \varepsilon\Gamma_T\left(\frac{\partial u}{\partial y}\right)^2(2-\gamma)\right]$$

Thus

$$Cf_x(Re_x)^{-\frac{1}{2}} = (1-\varepsilon)f'\prime(0) + \frac{\varepsilon}{2\sqrt{2}}We(f'\prime(0))^2(2-\gamma)$$

where,

$$Re_x = \frac{xU_e}{\nu} \; is \; the \; local \; Reynolds \; number.$$

3.2. Heat transfer rate

The local Nusselt Number is defined as:

$$Nu_x = \frac{xq_w}{k(T_w - T_\infty)}.$$

where, q_w symbolize surface heat flux and defined as:

$$q_w = -k\frac{\partial T}{\partial y} + q_r \; at \; y = 0.$$

Thus

$$Nu_x(Re_x)^{-\frac{1}{2}} = -\frac{2}{\sqrt{2-\beta}}\theta'(0)\left[1+\frac{4}{3R}[1+(\theta_w-1)(\theta(0))^3]\right].$$

3.3. Sherwood Number

The local Sherwood Number is interpreted as:

$$Sh_x = \frac{xJ_w}{D_B(C_w - C_\infty)}.$$

where, J_w represents surface mass flux and defined as:

$$J_w = -D_B \frac{\partial C}{\partial y} \ at \ y = 0.$$

Thus

$$Sh_x (Re_x)^{-\frac{1}{2}} = -\frac{2}{\sqrt{2-\beta}} \varphi^{'}(0).$$

3.4. Density number of micro-organisms distribution

The local density number of miro-organisms is defined as:

$$Nn_x = \frac{xP_w}{D_m (n - n_\infty)}.$$

where, P_w characterize motile micro-organisms flux and defined as:

$$P_w = -D_m \frac{\partial n}{\partial y} \ at \ y = 0. \tag{13}$$

Thus

$$Nn_x (Re_x)^{-\frac{1}{2}} = -\frac{2}{\sqrt{2-\beta}} \chi^{'}(0).$$

4. Solution procedure

This segment encloses numerical outcomes from the non-dimensional nonlinearly accompanying ordinary differential equations 8–11 with boundary conditions (12), that are integrated by utilizing RK-4 procedure. To achieve this analytical technique, the differential equations 8–11 are reduced into first order differential equation system, as displayed below:

$$q_1^{'} = q_2$$

$$q_2^{'} = q_3$$

$$q_3^{'} = \frac{1}{(1 + We^2 q_3^2)^{\frac{n-3}{2}} (1 + We^2 q_3^2) + (1-\varepsilon) + \frac{\varepsilon}{\sqrt{2}} (2 - \beta_T) W_T f^{''}} \left[- q_1 q_3 - \gamma (1 - q_2^2) + M(q_2 - 1) - \omega (q_4 - Nrq_6 - Rbq_8) \right]$$

$$q_4^{'} = q_5$$

$$q_5^{'} = \left(\frac{-1}{1 + \frac{4}{3R}(1 + q_4(\theta_w - 1))^3} \right) \left[Prq_1 q_5 + PrNbq_5 q_7 + PrNtq_5^2 + \frac{4}{R}(1 + q_4(\theta_w - 1))^2 (\theta_w - 1) q_5^2 + PrQq_4 \right]$$

$$q_6^{'} = q_7$$

$$q_7^{'} = -Leq_1 q_7 - \frac{Nt}{Nb} dq_5 + C_1 [1 + \delta q_4]^m exp \left[\frac{-E}{1 + \delta q_4} \right] q_6$$

$$q_8^{'} = q_9$$

$$q_9^{'} = -Lbq_1 q_9 + Pe[(\Omega_B + q_8) dq_7 + q_7 q_9]$$

along with the boundary conditions:

$$q_1 = V_0, \ q_2 = \lambda q_3^{'}(0), \ q_4 = 1 + \xi q_5(0), \ h_4^{'} = -1, \ q_6 = 1 + \beta q_7(0), \ q_8 = 1, \quad at \quad \eta = 0$$

$$q_2 \to 0, \ q_4 \to 0, \ q_6 \to 0, \ q_8 \to 0 \ as \ \eta \to \infty.$$

5. Results and discussion

In this assessment, the heat and mass transmission attributes of Carreau fluid and tangent hyperbolic fluid across a stretchable wedge are numerically evaluated while taking into account the magnetic field, slip situations, and non-variable heat flux. The results are exhibited graphically and in a tabular manner. Graphs depict the physical significance of the modulation of velocity, temperature, concentrations of nanoparticles and motile microorganisms for sundry parameters such as megnatic parameter M, suction parameter

V_0, mixed convection parameter ω, eigen value γ, Rayleigh number Rb, buoyancy ratio parameter Nr, thermal slip parameter ξ, Pr Prandtl number, Nb is Brownian motion parameter, Nt is thermophoresis parameter, radiation parameter Rd, heat source parameter Q, activation energy E, Chemical reaction parameter C_1, concentration slip parameter β, Lewis number Lb, microorganism concentration parameter Ω_B and Peclet number Pe. The range of distinct parameters while computing graphically is taken as $0.0 \leq M \leq 1.5$, $0.1 \leq V_0 \leq 1.0$, $0.1 \leq \gamma \leq 0.7$, $0.1 \leq \omega \leq 0.5$, $0.1 \leq Nr \leq 1.5$, $0.1 \leq Rb \leq 1.5$, $0.1 \leq Nt \leq 0.7$, $0.1 \leq Nb \leq 0.7$, $1.0 \leq Pr \leq 2.5$, $0.1 \leq Q \leq 0.4$, $2.0 \leq Rd \leq 3.5$, $0.0 \leq \xi \leq 0.5$, $0.1 \leq \theta_w \leq 1.0$, $3.0 \leq Le \leq 10.0$, $0.1 \leq E \leq 0.4$, $0.1 \leq C_1 \leq 0.7$, $0.01 \leq \beta \leq 0.07$, $0.5, \leq Lb \leq 2.0$, $0.1 \leq Pe \leq 0.25$ and $0.1 \leq \Omega_B \leq 1.5$.

To evaluate the accuracy of our computational framework, we contrast the present numerical values for $-f''(0)$ when V_0 is taken in range $[-1, 1]$ and other parameters are neglected to resemble with previous work of Ahmad and Khan [48], Ishak et al. [49], Postelnicu and Pop [50]. Table 1 reveals an acceptable accuracy between the current numerical results and the past studies. Table 2 exhibits that for both Carreau and tangent hyperbolic fluids, the skin friction coefficient $-f''(0)$ enhances notably with magnetic parameter M, suction parameter V_0, Eigen value γ, mixed convection parameter ω, but it lessens with buoyancy ratio parameter Nr and Rayleigh number Rb. Table 3 illustrates that the local Nusselt number $-\theta'(0)$ slightly decreases when Q, Nb and Nt are engaged, but it improves when R, Pr and θ_w are improved. Table 4 reveals that the local Sherwood number $-\varphi'(0)$ is explicitly enhanced directly with Le, Nt and C_1, but it shows meager increment for E and Nb. Table 5 signifies that when K, Pr and θ_w are given large inputs, the local motile density number $-\chi'(0)$ enhances dramatically whereas, the motile microorganisms density number $-\chi'(0)$ declines as Q, Nb and Nt get larger values.

To analyze the influences of distinct parameters on Tangent hyperbolic nanofluid, we fix $\varepsilon = 0.3$ and $We = 0.0$, while to probe the characteristics of Carreau fluid, we fix $We = 2.0$ and $\varepsilon = 0.0$. Fig. 2 depicts the implifications of magnetic parameter M and Suction parameter V_o on velocity distribution $f'(\eta)$ of both Tangent hyperbolic fluid and Carreau fluid. It can be detect that the uplifting values of M declines the velocity profile of both fluids. The velocity distribution declines because of an upsurge in drag force induced by gradually expanding values of the magnetic parameter M. It shows that the mounted values of V_o boosts the velocity of both the fluids. Fig. 3 examined the consequences of eigen value γ and mixed convection parameter ω on the velocity distribution for Carreau nanofluid and Tangent hyperbolic fluid which exhibit that the enlarging values of γ cause an increment in velocity of the both the fluids whereas, growing values of ω heightens the velocity of Carreau fluid and Tangent hyperbolic fluid. Physically, boosting the mixed convection variable ω induces the buoyancy force to overcome the inertial force, resulting in a dominating rise for $f'(\eta)$. Fig. 4 investigated the effects of the buoyancy ratio parameter Nr and Rayleigh number Rb on the velocity profile. The velocity is spotted to decline as the amount of Nr is boosted. It is basically defined as the existence of buoyancy forces provoke a decrement in velocity. Greater rates of natural and forced convection mashed thermal conductivity lessen rates of running along a permeable material for a massive stream of Carreau and Tangent hyperbolic nanofluids. It is mentionable that velocity for tangent hyperbolic fluid is faster than that of Carreau fluid. Similar effect is seen for Rb. Fig. 5 features the consequence of the Brownian motion parameter Nb and thermophoresis parameter Nt on a dimensionless temperature $\theta(\eta)$. When the values of Nb are intensified, it can be seen that the temperature of both fluids rises. As of the rapid diffusion rate of nanoparticles, heat transmission can be compensated for inducing the temperature to elevate. Although, the stronger Nt values correspond to higher temperatures. The movement of nanomaterials from a chilled destination to an elderly one is recognised as thermophoresis, and this tactic would improve the thermal variations as well. Fig. 6 depicts the discrepancy in temperature profiles for multiple larger values of the Prandtl number Pr as well as heat source parameter Q and the perception disempowering aspects in the heat flux of both liquids across the wedge, as the values of Pr boost, the thermal diffusivity tends to reduce, lowering the temperature. The heat source parameter Q is directly proportionate to the temperature field. As an outcome, the heat transfer in both Carreau and Tangent hyperbolic fluids tends to rise. Fig. 7 scrutinize the implifications of radiation parameter Rd, thermal slip parameter ξ and the temperature ratio parameter θ_w on the temperature distribution $\theta(\eta)$. It appears that enhancing Rd values elevate the temperature for both Carreau nanofluid and tangent hyperbolic fluid. This is due to the fact that introducing thermal radiation into the fluid increases the temperature and thickness of its boundary layer. The temperature variation of both fluids diminishes as the temperature slip parameter ξ boosts. This is due to the fact that as the values of ξ raise, so does the thickness of the thermal boundary layer. As the values of temperature ratio parameter θ_w upsurge, the temperature profile lessens. It is noticed that temperature for Carreau nanofluid is at higher level than that for tangent hyperbolic fluids. Fig. 8 explores the impacts of the Lewis number Le and activation energy E on the particle concentration $\varphi(\eta)$. The input values uncovered that enhancing the values of Le constrains concentration intensity for both liquids seeing as the Lewis number restricts fluid flow, whereas expanding the values of E boosts the concentration of nanomaterials. This attitude is clarified by the notion that as such of the minimal temperature and elevated activation, the rate of reaction is hindered, which enhances the concentration of the solution. As the worth of the chemical reaction parameter C_1 grows, the concentration boundary layer thickness shrinks, while the valuation of the concentration slip parameter β exceeds, the density of Carreau nanofluid and tangent hyperbolic fluid in the boundary surface

Table 1
The comparative outputs for V_0.

V_0	Ahmad and Khan [48]	Ishak et al. [49]	Postelnicu and Pop [50]	Present Results
−1.0	0.75650	0.7566	0.75657	0.7566
−0.5	0.96922	0.9692	0.96923	0.9692
0.0	1.23258	1.2326	1.2359	1.2326
0.5	1.54175	1.5418	1.5417	1.5417
1.0	1.88931	1.8893	1.8893	1.8893

Table 2
Results for $-f''(0)$.

V_0	M	γ	ω	Nr	Rb	Carreau Nanofluid	Tangent Hyperbolic Nanofluid
0.1	0.5	0.5	0.1	1.0	1.0	0.7205	0.3574
0.2						0.7402	0.3690
0.3						0.7601	0.3807
0.1	0.1					0.6517	0.3194
	0.5					0.7205	0.3574
	1.0					0.7945	0.3998
	0.5	0.1				0.5993	0.3564
		0.3				0.6638	0.3570
		0.5				0.7205	0.3574
		0.5	0.1			0.7205	0.3574
			0.2			0.7303	0.3631
			0.3			0.7397	0.3686
			0.1	0.1		0.7328	0.3645
				0.5		0.7274	0.3613
				1.0		0.7205	0.3574
				1.0	0.1	0.7500	0.3745
					0.5	0.7370	0.3669
					1.0	0.7205	0.3574

Table 3
Results for $-\theta'(0)$.

R	Pr	θ_w	Q	Nb	Nt	$-\theta'(0)$
2.0	1.0	1.1	0.5	0.1	0.1	0.6903
2.5						0.9175
3.0						1.1034
2.0	1.0					0.6903
	2.0					0.8513
	3.0					0.9336
	1.0	0.4				0.3401
		0.7				0.3595
		1.1				0.6903
		1.1	0.1			1.4730
			0.3			1.1264
			0.5			0.6903
			0.5	0.1		0.6903
				0.2		0.6691
				0.3		0.6483
				0.1	0.1	0.6903
					0.2	0.6707
					0.3	0.6512

Table 4
Results for Sherwood number $-\varphi'(0)$.

Le	Nb	Nt	E	C_1	$-\varphi'(0)$
3.0	0.1	0.1	1.0	0.5	5.3010
4.0					6.1469
5.0					6.9032
3.0	0.1				5.3010
	0.2				5.2778
	0.3				5.2473
	0.1	0.01			5.2266
		0.05			5.2596
		0.1			5.3010
		0.1	0.3		6.5148
			0.7		5.7825
			1.0		5.3010
			1.0	0.1	4.3156
				0.3	4.8839
				0.5	5.3010

Table 5
Results for local density number $-\chi'(0)$ of motile micro-organism.

Lb	*Pe*	Ω_B	$-\chi'(0)$
1.0	0.1	0.1	1.7125
2.0			2.2134
3.0			2.6210
1.0	0.1		1.7125
	0.2		2.2260
	0.3		2.7441
	0.1	0.1	1.7125
		0.2	1.7576
		0.3	1.8026

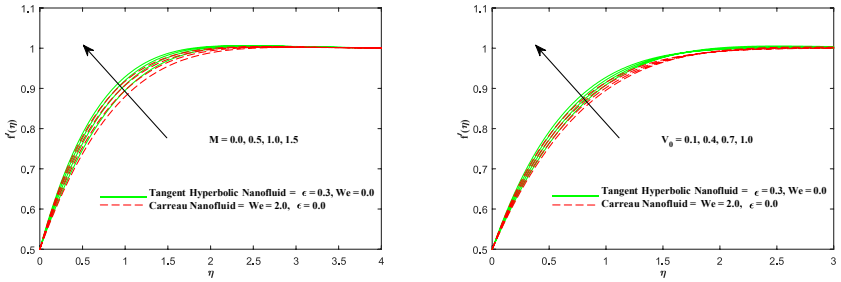

Fig. 2. Fluctuation in $f'(\eta)$ with M and V_0.

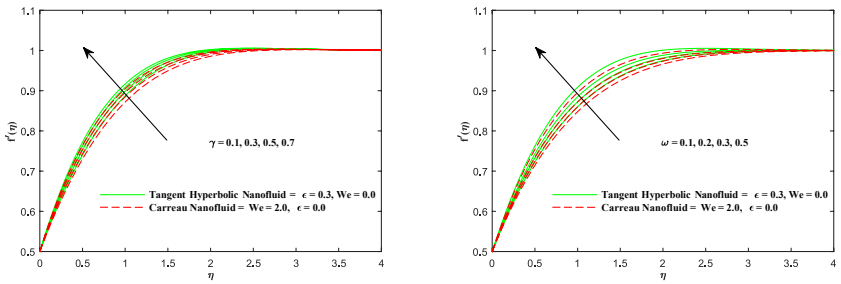

Fig. 3. Fluctuation in $f'(\eta)$ with γ and ω.

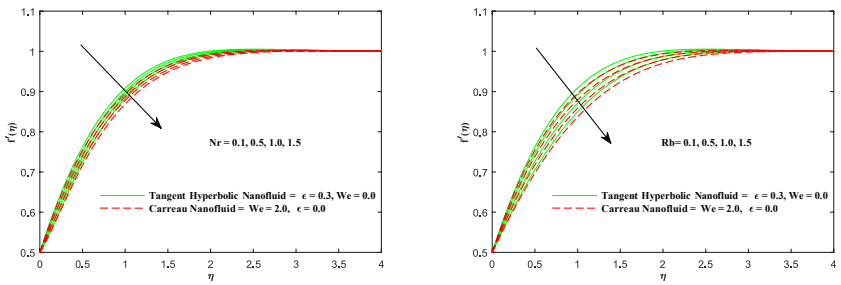

Fig. 4. Fluctuation in $f'(\eta)$ with *Nr* and *Rb*.

region declines as revealed in Fig. 9. The key reason is because as the chemical reaction parameter improves, the quantity of solute molecules enduring chemical reaction rises, causing a reduction in concentration field. As a result, a destructive chemical reaction significantly lowers the thickness of the solutal boundary layer. Fig. 10 depicts the implication of Brownian movement parameter *Nb* and thermophoresis parameter *Nt* on concentration delimitation layer texture. Surging values of *Nb* provoke the concentration patterns of the Carreau nanofluid and Tangent hyperbolic nanofluid to shrink in the flow region. The relationship between Brownian motion and Brownian dispersion factor, which is significant for minimising concentration field, is the origin of the reduction in concentration domain. Whereas, the mounting values of *Nt* trigger the thickness of the solutal fluid layers to accelerate. Thermophoresis behavior is frequently observed in several physical instances where heat transfer is more critical. Because of the greater heat close to the surface,

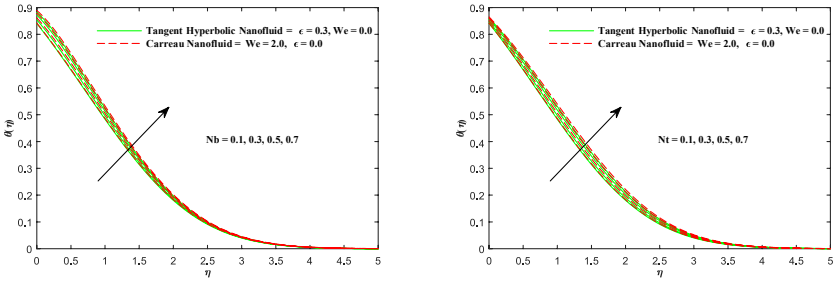

Fig. 5. Fluctuation in $\theta(\eta)$ with *Nb* and *Nt*.

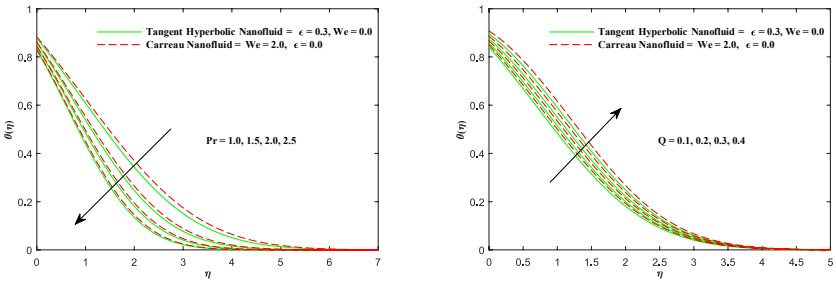

Fig. 6. Fluctuation in $\theta(\eta)$ with Pr and *Q*.

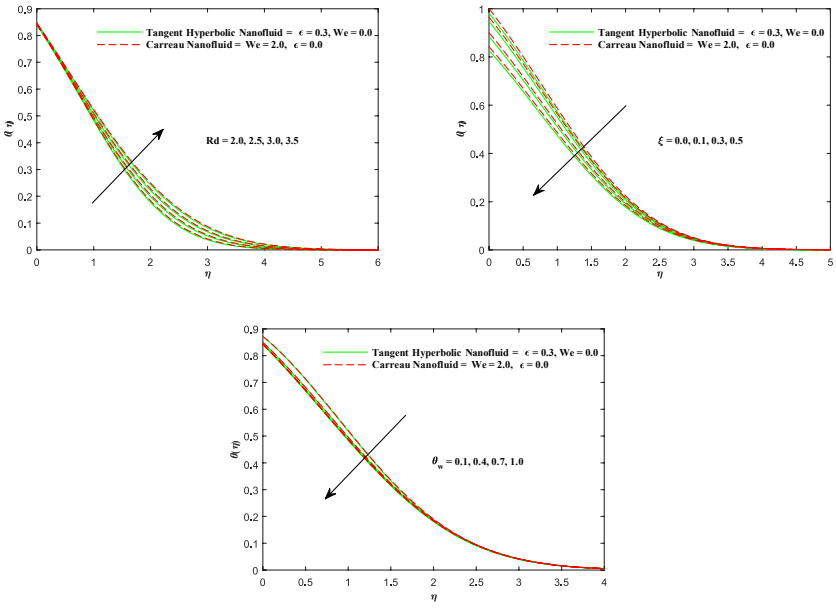

Fig. 7. Fluctuation in $\theta(\eta)$ with *Rd*, ξ and θ_w.

the liquid molecules flow to the relatively cool edge owing to the heat gradient and the concentration pattern improves as an outcome. Fig. 11 explores the consequences of Lewis number *Lb*, Peclet number *Pe* and microorganism concentration difference parameter Ω_B on motile density profile $\chi(\eta)$. The input values revealed that improving the values of Lb restricts motile density for both fluids because the Lewis number of bioconvection prevents fluids motion. Higher *Pe* values reduce the conductivity of microbes, and the deformation in the motile concentration of nanoparticles has been reviewed. The mountable values of Ω_B reduces the concentration of motile microbes as Ω_B is a significant parameter that infiltrates the motility of both Carreau and Tangent hyperbolic fluids.

6. Conclusions

The consequences of variational thermal radiation on the mass and heat transmission of Carreau and tangent hyperbolic nanofluid

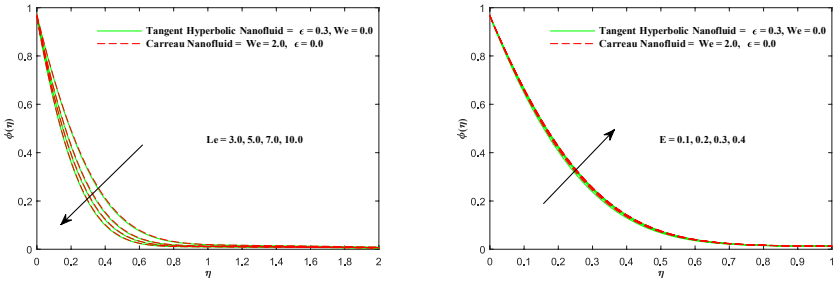

Fig. 8. Fluctuation in $\varphi(\eta)$ with *Le* and *E*.

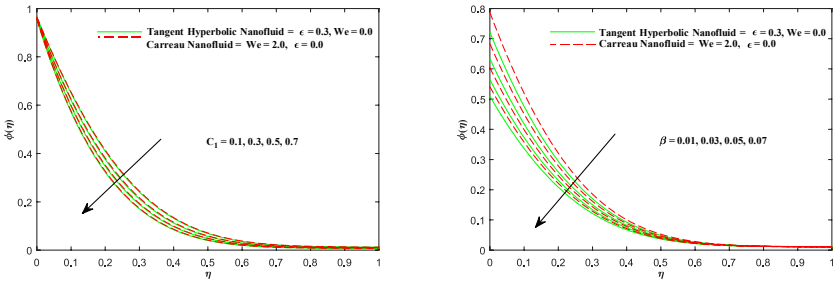

Fig. 9. Fluctuation in $\varphi(\eta)$ with C_1 and β.

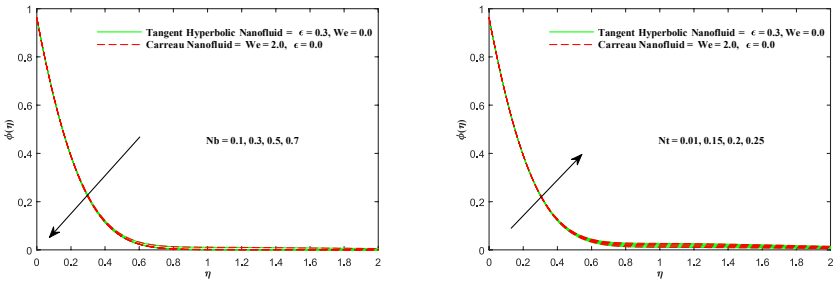

Fig. 10. Fluctuation in $\varphi(\eta)$ with *Nb* and *Nt*.

flows is stimulated due to stretchable wedge. The specific features encompass bio-convection, magnetic fields and thermal energy. The following are noteworthy outputs of the endeavour.

- Enhancing the inputs of *Nr* and *Rb* lessens $f'(\eta)$, but it strengthens as *M*, V_o, γ and ω values upsurge.
- Increased values of *Nt*, *Nb*, *Q* and *Rd* provoke an increment in heat distribution profile $\theta(\eta)$, so although risen values of *A*, ξ and θ_w lead to a reduction.
- The $\varphi(\eta)$ concentration behavior significantly reduces as the *Le*, C_1, β and *Nb* parameter values boost, even as the *E* and *Nt* parameters appreciably enhance the concentration.
- The motile density pattern of microbes $\chi(\eta)$ exhibits a notable reduction associated with high *Lb*, *Pe* and Ω_B values.
- The skin friction coefficient enhanced considerably with *M*, V_0, γ and ω, but dropped with an emerging tendency in *Nr* and *Rb* for both Carreau and Tangent Hyperbolic liquids.
- When the parameters *Nb*, *Nt* and *Q* are enhanced, the Nusselt number $-\theta'(0)$ drops considerably, so although it inflates for *R*, Pr and θ_w.
- As the parameters *Nb* and *E* are expanded, the Sherwood number $-\varphi'(0)$ shrinks, even though it grows for *Le*, *Nt* and C_1.
- The motile density number $-\chi'(0)$ deteriorates for *Lb*, *Pe* and Ω_B.

Future direction

In future, this work can be extended for hybrid nanofluid by using finite element method or finite volume method.

Acknowledgement

The authors extend their appreciation to Deanship of Scientific Research at King Khalid University, Saudi Arabia for funding this

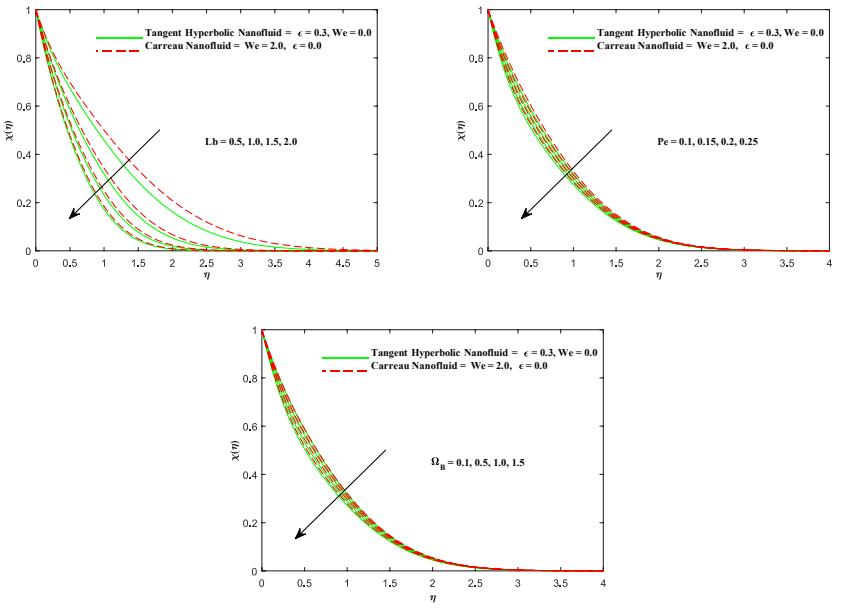

Fig. 11. Fluctuation in $\chi(\eta)$ with *Lb*, *Pe* and Ω.

work through large Groups Project under grant number R.G.P. 2/51/43.

Author statement

Dear Sir, all authors claimed that this work is original and neither submitted nor published anywhere. This work will be helpful for researcher and scientists. Also we claim that this work is suitable for this journal.

Declaration of competing interest

The authors declare that they have no known competing financial interests or personal relationships that could have appeared to influence the work reported in this paper.

Data availability

Data will be made available on request.

References

[1] M. Ramzan, H. Gul, S. Kadry, Y.-M. Chu, Role of bioconvection in a three dimensional tangent hyperbolic partially ionized magnetized nanofluid flow with cattaneo-christov heat flux and activation energy, Int. Commun. Heat Mass Tran. 120 (2021), 104994.
[2] M. Khan, A. Rasheed, T. Salahuddin, Radiation and chemical reactive impact on tangent hyperbolic fluid flow having double stratification, AIP Adv. 10 (7) (2020), 075211.
[3] K. Al-Khaled, S.U. Khan, I. Khan, Chemically reactive bioconvection flow of tangent hyperbolic nanoliquid with gyrotactic microorganisms and nonlinear thermal radiation, Heliyon 6 (1) (2020), e03117.
[4] K.G. Kumar, A. Baslem, B. Prasannakumara, J. Majdoubi, M. Rahimi-Gorji, S. Nadeem, Significance of arrhenius activation energy in flow and heat transfer of tangent hyperbolic fluid with zero mass flux condition, Microsyst. Technol. 26 (8) (2020) 2517–2526.
[5] P.P. Gharami, S. Reza-E-Rabbi, S. Arifuzzaman, M.S. Khan, T. Sarkar, S.F. Ahmmed, Mhd effect on unsteady flow of tangent hyperbolic nano-fluid past a moving cylinder with chemical reaction, SN Appl. Sci. 2 (7) (2020) 1–16.
[6] I.S. Oyelakin, P. Lalramneihmawii, S. Mondal, S.K. Nandy, P. Sibanda, Thermophysical analysis of three-dimensional magnetohydrodynamic flow of a tangent hyperbolic nanofluid, Eng. Rep. 2 (4) (2020), e12144.
[7] Z. Ullah, G. Zaman, A. Ishak, Magnetohydrodynamic tangent hyperbolic fluid flow past a stretching sheet, Chin. J. Phys. 66 (2020) 258–268.
[8] T. Karthik, K. Loganathan, A. Shankar, M.J. Carmichael, A. Mohan, M.K. Kaabar, S. Kayikci, Zero and nonzero mass flux effects of bioconvective viscoelastic nanofluid over a 3d riga surface with the swimming of gyrotactic microorganisms, Adv. Math. Phys. 2021 (2021) 1–13, https://doi.org/10.1155/2021/9914134.
[9] A. Mariam, I. Siddique, S. Abdal, F. Jarad, R. Ali, N. Salamat, S. Hussain, Bioconvection attribution for effective thermal transportation of upper convicted maxwell nanofluid flow due to an extending cylindrical surface, Case Stud. Therm. Eng. 34 (2022), 102062.
[10] I. Siddique, S. Abdal, I.S.U. Din, J. Awrejcewicz, W. Pawłowski, S. Hussain, Significance of concentration-dependent viscosity on the dynamics of tangent hyperbolic nanofluid subject to motile microorganisms over a non-linear stretching surface, Sci. Rep. 12 (1) (2022) 1–17.
[11] M. Khan, A. El Shafey, T. Salahuddin, F. Khan, Chemically homann stagnation point flow of carreau fluid, Phys. Stat. Mech. Appl. 551 (2020), 124066.
[12] S. Noreen, T. Kausar, D. Tripathi, Q.U. Ain, D. Lu, Heat transfer analysis on creeping flow carreau fluid driven by peristaltic pumping in an inclined asymmetric channel, Therm. Sci. Eng. Prog. 17 (2020), 100486.
[13] M. Khan, T. Salahuddin, E.-S.M. Sherif, H.S. Abdo, Wall slip characteristics on the dynamics of radioactive carreau fluid flow subjected to thermophysical properties of the rotating boundary layer, Int. Commun. Heat Mass Tran. 119 (2020), 104960.

[14] U. Nazir, S. Saleem, M. Nawaz, M.A. Sadiq, A. Alderremy, Study of transport phenomenon in carreau fluid using cattaneo–christov heat flux model with temperature dependent diffusion coefficients, Phys. Stat. Mech. Appl. 554 (2020), 123921.
[15] M. Madhu, B. Mahanthesh, N. Shashikumar, S. Shehzad, S. Khan, B. Gireesha, Performance of second law in carreau fluid flow by an inclined microchannel with radiative heated convective condition, Int. Commun. Heat Mass Tran. 117 (2020), 104761.
[16] M. Khan, A. Shahid, T. Salahuddin, M. Malik, A. Hussain, Analysis of two dimensional carreau fluid flow due to normal surface condition: a generalized fourier's and fick's laws, Phys. Stat. Mech. Appl. 540 (2020), 123024.
[17] A. Riaz, T. Abbas, A.Q. ul Ain, Nanoparticles phenomenon for the thermal management of wavy flow of a carreau fluid through a three-dimensional channel, J. Therm. Anal. Calorim. 143 (3) (2021) 2395–2410.
[18] M. Khan, T. Salahuddin, M. Malik, F. Khan, Change in internal energy of carreau fluid flow along with ohmic heating: a von karman application, Phys. Stat. Mech. Appl. 547 (2020), 123440.
[19] Z. Abdelmalek, S.U. Khan, H. Waqas, A. Riaz, I.A. Khan, I. Tlili, A mathematical model for bioconvection flow of williamson nanofluid over a stretching cylinder featuring variable thermal conductivity, activation energy and second-order slip, J. Therm. Anal. Calorim. 144 (2020) 1–13.
[20] M.Z. Ullah, T. Jang, An efficient numerical scheme for analyzing bioconvection in von-kármán flow of third-grade nanofluid with motile microorganisms, Alex. Eng. J. 59 (4) (2020) 2739–2752.
[21] D. Habib, N. Salamat, M. Ahsan, S. Abdal, I. Siddique, B. Ali, Significance of Bioconvection and Mass Transpiration for Mhd Micropolar Maxwell Nanofluid Flow over an Extending Sheet, Waves in Random and Complex Media, 2022, pp. 1–15.
[22] S. Abdal, I. Siddique, S. Afzal, S. Sharifi, M. Salimi, A. Ahmadian, An analysis for variable physical properties involved in the nano-biofilm transportation of sutterby fluid across shrinking/stretching surface, Nanomaterials 12 (4) (2022) 599.
[23] S. Abdal, I. Siddique, I.S.U. Din, A. Ahmadian, S. Hussain, M. Salimi, Significance of magnetohydrodynamic williamson sutterby nanofluid due to a rotating cone with bioconvection and anisotropic slip, ZAMM-J. Appl. Math. Mech.Zeitschrift für Angewandte Mathematik und Mechanik (2022), e202100503.
[24] D. Habib, N. Salamat, Z. Perveen, D. Alrowaili, S. Abdal, I. Siddique, A study on variable viscosity and activation energy for unsteady mhd bioconvection of nano fluid over a sheet with stretch and electric field, Comb. Chem. High Throughput Screen. (2022), https://doi.org/10.2174/1386207325666220414114228.
[25] S. Abdal, U. Habib, I. Siddique, A. Akgül, B. Ali, Attribution of multi-slips and bioconvection for micropolar nanofluids transpiration through porous medium over an extending sheet with pst and phf conditions, Int. J. Algorithm. Comput. Math. 7 (6) (2021) 1–21.
[26] S.U. Khan, K. Al-Khaled, A. Aldabesh, M. Awais, I. Tlili, Bioconvection flow in accelerated couple stress nanoparticles with activation energy: bio-fuel applications, Sci. Rep. 11 (1) (2021) 1–15.
[27] N. Shukla, P. Rana, S. Kuharat, O. Beg, Non-similar radiative bioconvection nanofluid flow under, Momentum 3 (2) (2021) 2.
[28] R. Koyama, L.-J. Chen, S. Alavi, R. Ohmura, Improving thermal efficiency of hydrate-based heat engine generating renewable energy from low-grade heat sources using a crystal engineering approach, Energy 198 (2020), 117403.
[29] X. Wang, H. Tian, F. Yan, W. Feng, R. Wang, J. Pan, Optimization of a distributed energy system with multiple waste heat sources and heat storage of different temperatures based on the energy quality, Appl. Therm. Eng. 181 (2020), 115975.
[30] K. Couvreur, W. Beyne, M. De Paepe, S. Lecompte, Hot water storage for increased electricity production with organic rankine cycle from intermittent residual heat sources in the steel industry, Energy 200 (2020), 117501.
[31] A. Jury, X. Balandraud, L. Heller, P. Šittner, M. Karlik, Reconstruction of heat sources induced in superelasticity loaded ni-ti wire by localized deformation processes, Exp. Mech. 61 (2) (2021) 349–366.
[32] W. Wang, M.M. Jaradat, I. Siddique, A.A.A. Mousa, S. Abdal, Z. Mustafa, H.M. Ali, On thermal distribution for Darcy–forchheimer flow of maxwell sutterby nanofluids over a radiated extending surface, Nanomaterials 12 (11) (2022) 1834.
[33] S. Abdal, I. Siddique, A. Ahmadian, S. Salahshour, M. Salimi, Enhanced heat transportation for bioconvective motion of maxwell nanofluids over a stretching sheet with cattaneo–christov flux, Mech. Time-Dependent Mater. (2022) 1–16.
[34] A. Raisi, S. Rostami, A.A. Nadooshan, M. Afrand, The examination of circular and elliptical vanes under natural convection of nanofluid in a square chamber subject to radiation effects, Int. Commun. Heat Mass Tran. 117 (2020), 104770.
[35] U. Ali, M. Malik, A. Alderremy, S. Aly, K.U. Rehman, A generalized findings on thermal radiation and heat generation/absorption in nanofluid flow regime, Phys. Stat. Mech. Appl. 553 (2020), 124026.
[36] B. Tamilzharasan, S. Karthikeyan, M.K. Kaabar, M. Yavuz, F. Özköse, Magneto mixed convection of williamson nanofluid flow through a double stratified porous medium in attendance of activation energy, Math. Comput. Appl. 27 (3) (2022) 46.
[37] D. Habib, N. Salamat, I. Siddique, Y. Hamed, K.M. Abualnaja, S. Abdal, S. Hussain, Role of Bioconvection, Porous Medium, and Activationenergy on the Dynamic of Sisko Nanofluid: the Case of Anenlarging Cylinder, Waves in Random and Complex Media, 2022, pp. 1–14.
[38] M. Bilal, Micropolar flow of emhd nanofluid with nonlinear thermal radiation and slip effects, Alex. Eng. J. 59 (2) (2020) 965–976.
[39] K.G. Kumar, E.H.B. Hani, M.E.H. Assad, M. Rahimi-Gorji, S. Nadeem, A novel approach for investigation of heat transfer enhancement with ferromagnetic hybrid nanofluid by considering solar radiation, Microsyst. Technol. 27 (1) (2021) 97–104.
[40] J. Raza, F. Mebarek-Oudina, P. Ram, S. Sharma, Mhd flow of non-Newtonian molybdenum disulfide nanofluid in a converging/diverging channel with rosseland radiation, Trans Tech Publ, Defect Diffusion Forum 401 (2020) 92–106.
[41] D.R. Hartree, On an equation occurring in falkner and skan's approximate treatment of the equations of the boundary layer, Cambridge University Press, Math. Proc. Camb. Phil. Soc. 33 (1937) 223–239.
[42] T. Kebede, E. Haile, G. Awgichew, T. Walelign, Heat and mass transfer analysis in unsteady flow of tangent hyperbolic nanofluid over a moving wedge with buoyancy and dissipation effects, Heliyon 6 (4) (2020), e03776.
[43] A. Hamid, M. Khan, A. Alshomrani, Non-linear radiation and chemical reaction effects on slip flow of williamson nanofluid due to a static/moving wedge: a revised model, Appl. Nanosci. 10 (8) (2020) 3171–3181.
[44] M. Siavashi, S. Iranmehr, Using sharp wedge-shaped porous media in front and wake regions of external nanofluid flow over a bundle of cylinders, Int. J. Numer. Methods Heat Fluid Flow 29 (2019) 3730–3755.
[45] P. Sreedevi, P.S. Reddy, M. Sheremet, A comparative study of al2o3 and tio2 nanofluid flow over a wedge with non-linear thermal radiation, Int. J. Numer. Methods Heat Fluid Flow 30 (2020) 1291–1317.
[46] K. Jyothi, P.S. Reddy, M.S. Reddy, Carreau nanofluid heat and mass transfer flow through wedge with slip conditions and nonlinear thermal radiation, J. Braz. Soc. Mech. Sci. Eng. 41 (10) (2019) 1–15.
[47] A. Patra, M. Nayak, A. Misra, Effects of non-uniform suction, heat generation/absorption and chemical reaction with activation energy on mhd falkner-skan flow of tangent hyperbolic nanofluid over a stretching/shrinking eedge, J. Comput. Appl. Mech. 6 (3) (2020) 640–652.
[48] R. Ahmad, W.A. Khan, Effect of viscous dissipation and internal heat generation/absorption on heat transfer flow over a moving wedge with convective boundary condition, Heat Tran. Asian Res. 42 (7) (2013) 589–602.
[49] A. Ishak, R. Nazar, I. Pop, Falkner-skan equation for flow past a moving wedge with suction or injection, J. Appl. Math.Comput. 25 (1) (2007) 67–83.
[50] A. Postelnicu, I. Pop, Falkner–skan boundary layer flow of a power-law fluid past a stretching wedge, Appl. Math. Comput. 217 (9) (2011) 4359–4368.